SCIENTIFIC REPORTS

OPEN

Growth of single-crystalline Bi_2Te_3 hexagonal nanoplates with and without single nanopores during temperature-controlled solvothermal synthesis

Received: 8 January 2019
Accepted: 16 July 2019
Published online: 25 July 2019

Yuichi Hosokawa[1], Koji Tomita[2] & Masayuki Takashiri[1]

Bismuth telluride (Bi_2Te_3) is a promising thermoelectric material for applications near room temperature. To increase the thermoelectric performance of this material, its dimensions and thermal transport should be decreased. Two-dimensional nanoplates with nanopores are an ideal structure because thermal transport is disrupted by nanopores. We prepared Bi_2Te_3 nanoplates with single nanopores by a solvothermal synthesis and investigated their structural and crystallographic properties. The nanoplates synthesized at a lower reaction temperature (190 °C) developed single nanopores (approximately 20 nm in diameter), whereas the nanoplates synthesized at a higher reaction temperature (200 °C) did not have nanopores. A crystal growth mechanism is proposed based on the experimental observations.

Bismuth telluride (Bi_2Te_3) has attracted intense attention as a functional material in applications such as traditional thermoelectric systems[1,2], three-dimensional (3D) topological insulators[3,4], and photovoltaic materials[5]. The crystal structure of Bi_2Te_3 is a rhombohedral tetradymite-type with the space group R-3m, and is described by a hexagonal unit cell, as shown in Fig. 1. The unit cell is composed of five covalently bonded monatomic sheets along the *c*-axis in the sequence –Te(1)–Bi–Te(2)–Bi–Te(1)–Te(1)–Bi–Te(2)–Bi–Te(1)–. Here, (1) and (2) denote two different chemical states of the anions. The nature of the bonding between neighboring Te(1) layers is a weak van der Waals attraction, whereas the bonding between bismuth and tellurium atoms is mainly covalent with a small ionic contribution. Because of this crystal structure, the lattice constant of the *c*-axis (3.045 nm) is approximately seven times as large as that of the *a*, *b*-axis (0.438 nm), leading to remarkable anisotropic behavior[6–8].

Recently, nanosized Bi_2Te_3 materials have been shown to exhibit excellent thermoelectric performance[9]. This high performance is mainly attributed to the effects of the low dimensionality and the reduction of the lattice thermal conductivity at phonon scattering centers[10–12]. Among various shapes of nanosized Bi_2Te_3 materials, including nanoplates[13–15], nanoparticles[16–18], and nanocrystalline films[19–22], nanoplates are the most appropriate shape to take advantage of the inherent features of the Bi_2Te_3 crystal structure. This is because Bi_2Te_3 nanoplates are single-crystalline and have a hexagonal shape similar to that of the unit cell. To prepare Bi_2Te_3 nanoplates, solvothermal and hydrothermal syntheses are the most practical methods because of their cost efficiency and simplicity. In these syntheses, a precursor solution is placed in a pressure vessel and heated to temperatures much higher than their normal boiling points to enhance the chemical reaction and yield nanoplates. The difference between the solvothermal and hydrothermal syntheses is whether the precursor solution is non-aqueous (solvo) or aqueous (hydro).

Bi_2Te_3 nanoplates with a hexagonal shape are generally synthesized by solvothermal methods[23,24]. Typical Bi_2Te_3 nanoplates take the shape of a regular hexagon and have atomically flat surfaces[25,26]. Thermoelectric performance can be increased by forming optimized nanopores in the material, which decrease the thermal conductivity while preserving the electrical properties[27]. Therefore, if nanopores are formed in nanoplates, the

[1]Department of Materials Science, Tokai University, 4-1-1 Kitakaname, Hiratsuka, Kanagawa, 259-1292, Japan. [2]Department of Chemistry, Tokai University, 4-1-1 Kitakaname, Hiratsuka, Kanagawa, 259-1292, Japan. Correspondence and requests for materials should be addressed to M.T. (email: takashiri@tokai-u.jp)

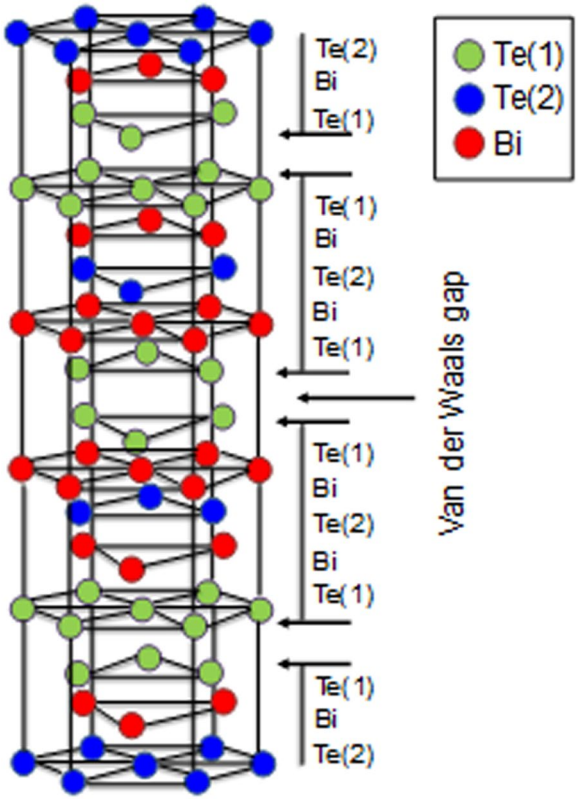

Figure 1. Schematic crystal structure of Bi_2Te_3.

thermoelectric performance of the nanoplates might be expected to further increase. However, to the best of our knowledge, there have been no reports on the crystal growth of Bi_2Te_3 nanoplates containing nanopores.

In this study, we prepare Bi_2Te_3 hexagonal nanoplates with single nanopores based on a solvothermal synthesis. For comparison, Bi_2Te_3 hexagonal nanoplates with no nanopores were also prepared using solvothermal synthesis by changing the reaction temperature. The structural and crystallographic characteristics of the nanoplates were investigated. On the basis of our experimental observations and understanding of the crystal growth, the formation of the nanoplates with nanopores is discussed.

Methods

Single-crystalline Bi_2Te_3 hexagonal nanoplates were formed in a solvothermal synthesis. The basic experimental method has been described in our previous work[28,29]. The nanoplates were prepared in a Teflon-container within a stainless-steel autoclave, involving a reaction under high pressure and high temperature. Stirring was applied with a hot plate and magnetic stirrer. Bi_2O_3 (Fujifilm Wako Pure Chemical Co., >99.9%) and TeO_2 (Kojundo Chemical Laboratory Co., Ltd., >99.9%) were used as Bi_2Te_3 sources, and $C_2H_6O_2$ (Fujifilm Wako Pure Chemical Co., >90.0%) was used as a ligand. NaOH (Fujifilm Wako Pure Chemical Co., >97.0%) and polyvinyl pyrrolidone (Fujifilm Wako Pure Chemical Co., K30, M_s ~40,000) were contained in the solution. All chemicals were used as received without further purification. The Bi_2Te_3 nanoplates were synthesized according to the following procedure: 0.4 g of PVP was dissolved in ethylene glycol (18 mL), followed by the addition of Bi_2O_3 (0.02 mol/L), TeO_2 (0.07 mol/L), and 2 mL of a NaOH solution (5.0 mol/L). The resulting precursor solution was sealed in the autoclave and heated and maintained at either 190 °C or 200 °C for 4 h with magnetic stirring at 500 rpm. After the synthesis, the products were allowed to cool down below 50 °C naturally. The residue was washed several times with distilled water and absolute ethanol and the products were collected by centrifugation. Finally, the products were dried under vacuum at 60 °C for 24 h.

We analyzed the microstructure of Bi_2Te_3 nanoplates with a field emission scanning electron microscope (FE-SEM, Hitachi S-4800). The precise structure of the nanoplates was analyzed with a high-resolution transmission electron microscope (TEM, JEOL JEM-ARM200F) and selected area electron diffraction (SAED) at an accelerating voltage of 200 kV. The chemical composition of the nanoplates was determined with an electron probe microanalyzer (EPMA, Shimadzu EPMA-1610). The compositions of the samples were calibrated using the ZAF4 program installed with the EPMA-1610. X-ray diffraction (XRD, Rigaku MiniFlex600) analyses were performed to determine the crystal lattice structure and the phase purity of the nanoplates. We used Cu-Kα radiation at a scanning rate of 0.02°/s over the 2θ range of 10° to 80°.

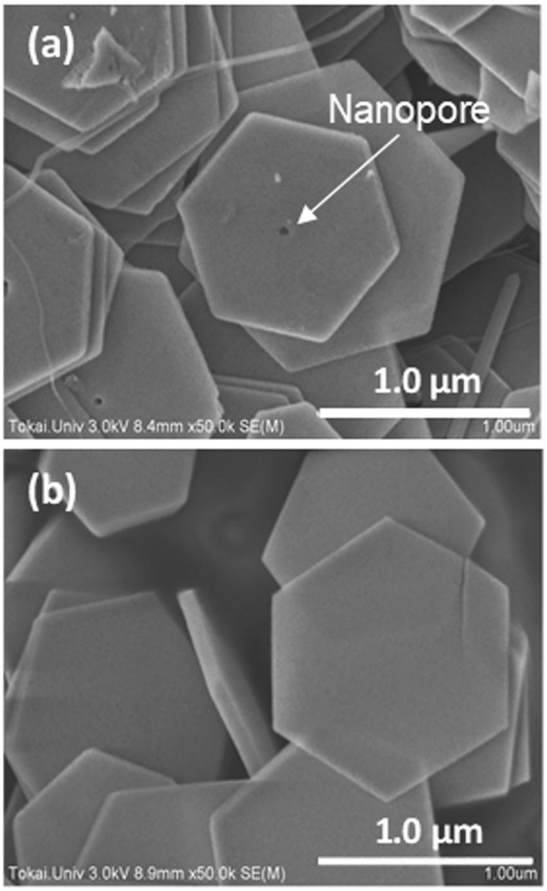

Figure 2. SEM images of the Bi_2Te_3 nanoplates synthesized at (**a**) 190 °C and (**b**) 200 °C.

Results and Discussion

Figure 2 shows SEM images of the Bi_2Te_3 nanoplates formed at different reaction temperatures in the solvothermal synthesis. At a reaction temperature of 190 °C (Fig. 2(a)), we obtained hexagonal nanoplates with edge lengths of approximately 1 μm. A single nanopore appeared in the center of the nanoplates. We also observed several samples manufactured under the same conditions as the sample shown in the SEM image and found a nanopore in the center of almost every nanoplate (The detailed information is provided in Fig. S1). Hence, the nanopores were naturally generated in the crystal growth process and not caused by accidental collisions between the nanoplates. At a reaction temperature of 200 °C (Fig. 2(b)), the nanoplates had a similar edge length of approximately 1 μm but no nanopores were observed. We also fabricated Bi_2Te_3 nanoplates at reaction temperatures of 180 °C and 230 °C, and observed their surface morphologies using FE-SEM (The detailed information is provided in Fig. S2). As a result, single nanopores were obtained in the nanoplates at 180 °C, but not in those formed at 230 °C. Therefore, we conclude that the synthesis at relatively low reaction temperatures yielded nanoplates with single nanopores and the nanopores disappeared as the reaction temperature was increased.

To further investigate the precise structure of the Bi_2Te_3 nanoplates, we performed TEM observations, as shown in Fig. 3. The TEM images of the Bi_2Te_3 nanoplates synthesized at a reaction temperature of 190 °C are shown in Fig. 3(a). The nanoplates had sharp edges with a distance of approximately 1 μm between the opposite edges, and a very smooth surface, which indicated excellent crystallinity. The mesh structure behind the nanoplate was visible indicating the low thickness of the plate. The size of the nanopores was approximately 20 nm, and each was located close to the center of each nanoplate. Figure 3(b) shows high-resolution TEM (HRTEM) images of the nanoplates near the nanopores. The SAED pattern inset in Fig. 3(b) shows a hexagonal symmetry diffraction spot pattern, which indicates its single-crystalline nature. Lattice fringes cannot be seen in the range of approximately 5 nm from the nanopore, suggesting an amorphous structure in this region. However, clear lattice fringes were observed in this region at distances greater than 5 nm from the edges of the nanopores. The lattice fringes were structurally uniform with a spacing of 0.21 nm, which is in good agreement with the d values of the (110) planes of rhombohedral Bi_2Te_3. From Fig. 3(a,b), we conclude that single-crystal nanoplates grew along the (00*l*) planes except for regions near the nanopores. Figure 3(c) shows a TEM image of a Bi_2Te_3 nanoplate synthesized at a reaction temperature of 200 °C. The shape of the nanoplate was almost the same as that synthesized at 190 °C except for the presence of the nanopore. The HRTEM image in Fig. 3(d) clearly shows that the lattice fringes were also structurally uniform with a spacing of 0.21 nm, which is in good agreement with the d value of the (110) planes of rhombohedral Bi_2Te_3. The SAED pattern shown in the inset of Fig. 3(d) was indexed to the [00*l*] zone axis of rhombohedral Bi_2Te_3, indicating that this nanoplate was single-crystalline and had a preferential

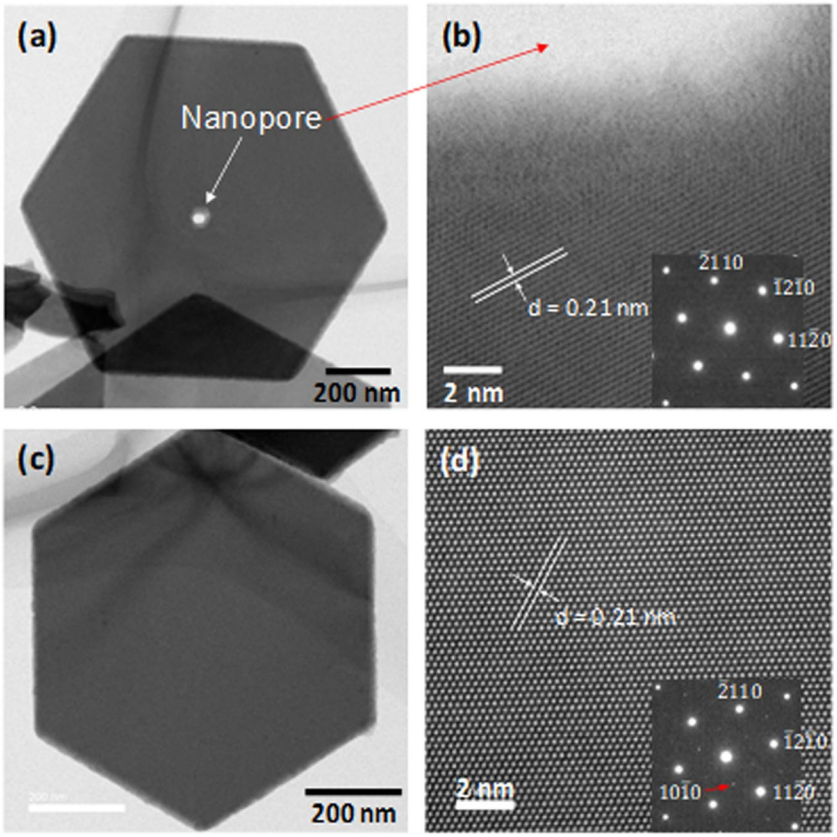

Figure 3. (**a**) TEM image of Bi_2Te_3 nanoplate with a single nanopore synthesized at 190 °C. (**b**) Corresponding SAED pattern and HRTEM image of the nanoplate in (**a**). (**c**) TEM image of Bi_2Te_3 nanoplate synthesized at 200 °C. (**d**) Corresponding SAED pattern and HRTEM image of the nanoplate in (**c**).

Reaction temperature (°C)	Atomic composition ratio Te/(Bi + Te)
190	0.56
200	0.54

Table 1. Atomic composition ratio of the Bi_2Te_3.

(00*l*) orientation. Notably, weak forbidden reflections were observed, owing to the broken translational symmetry of the Te/Bi antisite defects, which is consistent with previous reports[28,30,31].

The atomic composition ratios [Te/(Bi + Te)] of the Bi_2Te_3 nanoplates prepared at different reaction temperatures are listed in Table 1. The composition ratio of the nanoplates with single nanopores formed at 190 °C was 0.56, which is slightly lower than the stoichiometric proportion of 0.6. At a reaction temperature of 200 °C, the composition ratio of the nanoplates was 0.54. This result gives insight into the behavior of Te/Bi antisite defects, as shown in Fig. 3(d). The composition ratio of the nanoplates with no nanopores was lower than that of the nanoplates with nanopores; thus, a relatively large amount of Te atoms replaced Bi atoms in the nanoplates without nanopores.

The phase purity and crystal structure of the Bi_2Te_3 nanoplates were examined by XRD analysis, as shown in Fig. 4. All peaks observed in the XRD patterns of the nanoplates formed at reaction temperatures of 190 °C and 200 °C were indexed to the standard diffraction pattern of Bi_2Te_3 (JCPDS 15-0863) although both nanoplates exhibited slight deviations from the exact stoichiometry. The main peaks originated from the (006), (015), (10 10), and (00 15) planes. Therefore, the phase purity and the crystal structure depended only slightly on nanopores in the Bi_2Te_3 nanoplates.

As mentioned above, the single nanopores appeared at the centers of the single-crystalline Bi_2Te_3 hexagonal nanoplates at the lower reaction temperature. Here, we propose a growth mechanism and reaction process to account for the structures of these nanoplates. Figure 5 shows a schematic diagram of the crystal growth of the nanoplates with and without single nanopores. When Bi_2Te_3 nuclei were generated in the solution, they aggregated. The atomic composition ratios of the nanoplates synthesized at different temperatures deviated slightly from the stoichiometric proportion; however, we consider that this deviation did not affect the aggregation process of the nuclei and Ostwald ripening process described below. When the radius of the aggregated nuclei

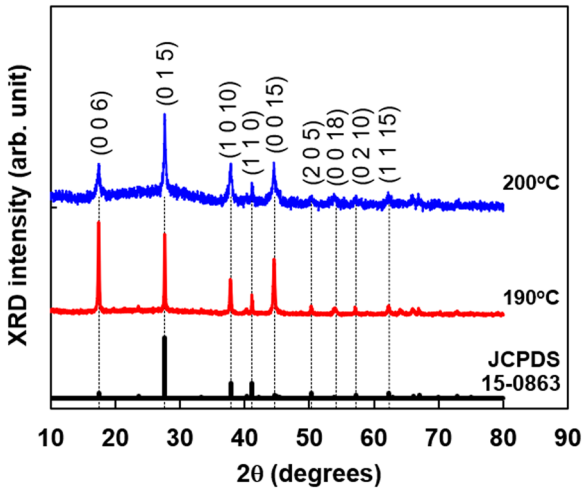

Figure 4. X-ray diffraction patterns of the Bi_2Te_3 nanoplates prepared by solvothermal synthesis (**a**) with and (**b**) without nanopores.

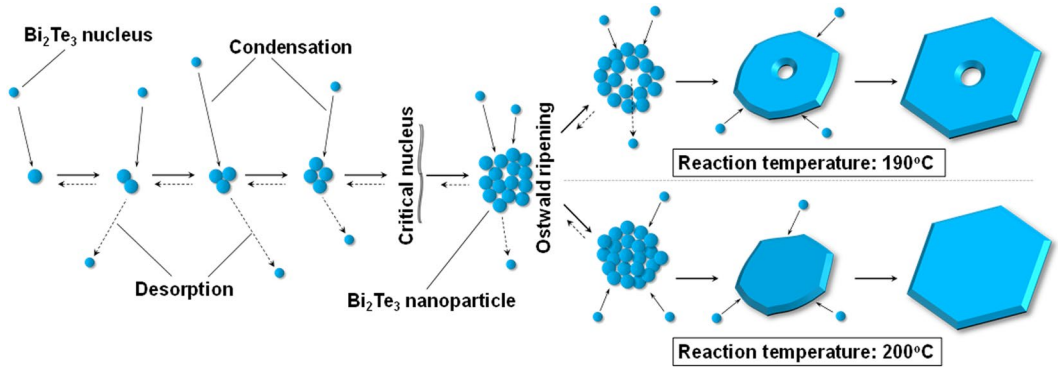

Figure 5. Schematic diagram of the crystal growth of nanoplates with and without single nanopores.

became larger than the critical nucleus, Bi_2Te_3 nanoparticles were generated. In the Bi_2Te_3 system, the formation of nanoplates is also attributed to the inherent crystal structure. Because of the high surface energy of the nuclei, the aggregated Bi_2Te_3 particles were not in thermodynamic equilibrium and were metastable; Bi_2Te_3 nanoplates with a thermodynamic preference for better crystallinity. After formation of Bi_2Te_3 nanoplates, the Ostwald ripening process proceeded; however, the process differed at reaction temperatures of 190 °C and 200 °C[32]. At a reaction temperature of 190 °C, Ostwald ripening led to the formation of nanopore structures because of lower crystallinity or less dense particles in the colloidal aggregate, which gradually dissolved, whereas larger, better crystallized or denser particles in the same aggregate continued to grow at the lower reaction temperature. However, at 200 °C, nanopores were not formed in the nanoplates because the particles in the colloidal aggregate did not dissolve owing to the dense structures initially formed at the higher reaction temperature. Both types of Bi_2Te_3 nanoplates grew gradually to form deep nanoplates with many crystalline planes from the top to bottom[33,34]. Rhombohedral Bi_2Te_3 is built up from many layers extending along the top-to-bottom crystalline planes connected by van der Waals bonds, as shown in Fig. 1.

Conclusions

We used solvothermal synthesis at different reaction temperatures to prepare Bi_2Te_3 hexagonal nanoplates. The structural and crystallographic characteristics of the nanoplates were investigated. The nanoplates synthesized at a lower reaction temperature (190 °C) developed single nanopores (approximately 20 nm in diameter), whereas the nanoplates synthesized at a higher reaction temperature (200 °C) did not have nanopores. Based on the experimental and analytical results, we propose a growth mechanism and reaction process for the nanoplates and the nanopore appearance at different reaction temperatures. We expect that the Bi_2Te_3 nanoplates with single nanopores will feature improved thermoelectric performance.

References

1. Goldsmid, H. J. & Douglas, R. W. The use of semiconductors in thermoelectric refrigeration. *Br. J. Appl. Phys.* **5**, 386–390 (1954).
2. Scherrer, H. & Scherrer, S. In *CRC Handbook of Thermoelectrics*, ed. by Rowe, D. M., CRC Press, Boca Raton, Sec. D, pp. 211–238 (1995).
3. Chen, Y. L. *et al*. Experimental realization of a three-dimensional topological insulator. *Bi2Te3, Science* **325**, 178–181 (2009).

4. Hsieh, D. *et al*. Observation of time-reversal-protected single-dirac-cone topological-insulator states in Bi_2Te_3 and Sb_2Te_3. *Phys. Rev. Lett.* **103**, 146401 (2009).
5. Liu, Y. *et al*. Bulk photovoltaic effect at infrared wavelength in strained Bi_2Te_3 films. *APL Mater.* **4**, 126104 (2016).
6. Kaibe, H., Tanaka, Y., Sakata, M. & Nishida, I. Anisotropic galvanomagnetic and thermoelectric properties of n-type Bi_2Te_3 single crystal with the composition of a useful thermoelectric cooling material. *J. Phys. Chem. Solids* **50**, 945–950 (1989).
7. Yamauchi, K. & Takashiri, M. Highly oriented crystal growth of nanocrystalline bismuth telluride thin films with anisotropic thermoelectric properties using two-step treatment. *J. Alloys Compd.* **698**, 977–983 (2017).
8. Kudo, S., Tanaka, S., Miyazaki, K., Nishi, Y. & Takashiri, M. Anisotropic analysis of nanocrystalline bismuth telluride thin films treated by homogeneous electron beam irradiation. *Mater. Trans.* **58**, 513–519 (2017).
9. Venkatasubramanian, R., Siivola, E., Colpitts, T. & O'Quinn, B. Thin-film thermoelectric devices with high room-temperature figures of merit. *Nature* **413**, 597–602 (2001).
10. Hicks, L. D. & Dresselhaus, M. S. Effect of quantum-well structure on the thermoelectric figure of merit. *Phys. Rev. B* **47**, 12727 (1993).
11. Poudel, B. *et al*. High-thermoelectric performance of nanostructured bismuth antimony telluride bulk alloys. *Science* **320**, 634–638 (2008).
12. Takashiri, M. *et al*. Effect of grain size on thermoelectric properties of n-type nanocrystalline bismuth-telluride based thin films. *J. Appl. Phys.* **104**, 084302 (2008).
13. Fan, X. A. *et al*. Bi_2Te_3 hexagonal nanoplates and thermoelectric properties of n-type Bi_2Te_3 nanocomposites. *J. Phys. D: Appl. Phys.* **40**, 5975–5979 (2007).
14. Hosokawa, Y., Wada, K., Tanaka, M., Tomita, K. & Takashiri, M. Thermal annealing effect on structural and thermoelectric properties of hexagonal Bi2Te3 nanoplate thin films by drop-casting technique. *Jpn. J. Appl. Phys.* **57**, 02CC02 (2018).
15. Xu, Y. *et al*. Synthesis of single crystal Bi_2Te_3 nanoplates via an inorganic-surfactant-assisted solvothermal route. *Mater. Lett.* **62**, 4525–4528 (2008).
16. Xie, K. *et al*. Quasi continuous wave laser sintering of Si-Ge nanoparticles for thermoelectrics. *J. Appl. Phys.* **123**, 094301 (2018).
17. Takashiri, M. *et al*. Preparation and characterization of $Bi_{0.4}Te_{3.0}Sb_{1.6}$ nanoparticles and their thin films. *J. Alloys Compd.* **462**, 351–355 (2008).
18. Takashiri, M., Tanaka, S. & Miyazaki, K. Growth of single-crystalline bismuth antimony telluride nanoplates on the surface of nanoparticle thin films. *J. Cryst. Growth* **372**, 199–204 (2013).
19. Liao, C.-N., Wang, Y.-C. & Chu, H.-S. Thermal transport properties of nanocrystalline Bi–Sb–Te thin films prepared by sputter deposition. *J. Appl. Phys.* **104**, 104312 (2008).
20. Takashiri, M., Takiishi, M., Tanaka, S., Miyazaki, K. & Tsukamoto, H. Thermoelectric properties of n-type nanocrystalline bismuth-telluride-based thin films deposited by flash evaporation. *J. Appl. Phys.* **101**, 074301 (2007).
21. Kudo, S., Hagino, H., Tanaka, S., Miyazaki, K. & Takashiri, M. Determining the thermal conductivity of nanocrystalline bismuth telluride thin films using the differential 3ω method while accounting for thermal contact resistance. *J. Electron. Mater.* **44**, 2021–2025 (2015).
22. Morikawa, S., Satake, Y. & Takashiri, M. Characteristics of nanostructured bismuth telluride thin films fabricated by oblique deposition. *Vacuum* **148**, 296–302 (2018).
23. Wada, K., Tomita, K. & Takashiri, M. Thermoelectric properties of bismuth telluride nanoplate thin films determined using combined infrared spectroscopy and first-principles calculation. *Jpn. J. Appl. Phys.* **57**, 06HC02 (2018).
24. Son, J. S. *et al*. N-type nanostructured thermoelectric materials prepared from chemically synthesized ultrathin Bi_2Te_3 nanoplates. *Nano Lett.* **12**, 640–647 (2012).
25. Hao, G. *et al*. Growth and surface potential characterization of Bi_2Te_3 nanoplates. *AIP Adv.* **2**, 012114 (2012).
26. Zhang, Y., Hu, L. P., Zhu, T. J., Xie, J. & Zhao, X. B. High yield Bi_2Te_3 single crystal nanosheets with uniform morphology via a solvothermal synthesis. *Cryst. Growth Des.* **13**, 645–651 (2013).
27. Kashiwagi, M. *et al*. Enhanced figure of merit of a porous thin film of bismuth antimony telluride. *Appl. Phys. Lett.* **98**, 023114 (2011).
28. Takashiri, M., Kai, S., Wada, K., Takasugi, S. & Tomita, K. Role of stirring assist during solvothermal synthesis for preparing single-crystal bismuth telluride hexagonal nanoplates. *Mater. Chem. Phys.* **173**, 213–218 (2016).
29. Wada, K., Tomita, K. & Takashiri, M. Fabrication of bismuth telluride nanoplates via solvothermal synthesis using different alkalis and nanoplate thin films by printing method. *J. Cryst. Growth* **468**, 194–198 (2017).
30. Kong, D. *et al*. Few-layer nanoplates of Bi_2Se_3 and Bi_2Te_3 with highly tunable chemical potential. *Nano Lett.* **10**, 2245–2250 (2010).
31. Mehta, R. J. *et al*. A new class of doped nanobulk high-figure-of-merit thermoelectrics by scalable bottom-up assembly. *Nat. Mater.* **11**, 233–240 (2012).
32. Voorhees, P. W. The theory of Ostwald ripening *J. Stat. Phys.* **38**, 231–252 (1985).
33. Jin, R., Chen, G., Pei, J., Xu, H. & Lv, Z. S. Solvothermal synthesis and growth mechanism of ultrathin Sb_2Te_3 hexagonal nanoplates with thermoelectric transport properties. *RSC Adv.* **2**, 1450–1456 (2012).
34. Zhang, G., Wang, W., Lu, X. & Li, X. Solvothermal synthesis of V–VI binary and ternary hexagonal platelets: the oriented attachment mechanism. *Cryst. Growth Des.* **9**, 145–150 (2009).

Acknowledgements

This study was partly supported by the Japan Society for the Promotion of Science (JSPS) KAKENHI [Grant Number 16K06752]. A part of this study was conducted at Hokkaido University, supported by "Nanotechnology Platform" Program of the Ministry of Education, Culture, Sports, Science and Technology (MEXT), Japan. The authors wish to thank N. Nakazato, M. Takahashi, A. Kobayashi, S. Yonezawa, H. Yabuki, and S. Tsuda for providing experimental support. We thank Andrew Jackson, PhD, from Edanz Group (www.edanzediting.com/ac) for editing a draft of this manuscript.

Author Contributions

M.T. and K.T. gestated the idea and designed the experiments. Y.H. and M.T. completed the main manuscript text. The experiments and data analysis were conducted by Y.H. with help from M.T. and K.T. All the authors discussed the results and commented on the manuscript.

Additional Information

Supplementary information accompanies this paper at https://doi.org/10.1038/s41598-019-47356-5.

Competing Interests: The authors declare no competing interests.

Publisher's note: Springer Nature remains neutral with regard to jurisdictional claims in published maps and institutional affiliations.